JrnlID 12520_ArtID 1041_Proof# 1 - 04/03/2020

Archaeological and Anthropological Sciences _####################_
https://doi.org/10.1007/s12520-020-01041-1

ORIGINAL PAPER

New constraints on the medieval repopulation process in the northern Iberian plateau from the full vector archaeomagnetic dating of two hearths at La Pudia site (Caleruega, Burgos, Spain)

N. García-Redondo[1] · Á. Carrancho[2] · A. Goguitchaichvili[3] · J Morales[3] · M. Calvo-Rathert[1] · Á. Palomino[4]

Received: 30 September 2019 / Accepted: 25 February 2020

Abstract
The progressive southward reoccupation of territories of the Iberian Peninsula by the Christian kingdom against the Muslims from the eighth century AD onwards is a well-known process. However, there are few well-dated sites of this period, especially in the northern plateau of Spain. Here we report the full vector archaeomagnetic dating of two hearths from the archaeological site of La Pudia I (Caleruega, Castile-and-León, Spain). Both hearths were archaeomagnetically investigated in order to date their last use linked to the abandonment of the site. The archaeomagnetic direction was analysed through thermal (TH) and stepwise alternating field (AF) demagnetization of the natural remanent magnetization (NRM). Pseudo-single domain slightly substituted magnetite was identified as the main magnetic carrier. Thellier–Coe type absolute archaeointensity determinations were carried out on 48 samples from both hearths. The mean directions obtained were independently analysed both at sample and at specimen levels yielding very similar results but statistically distinguishable at 95% confidence level. The archaeomagnetic dating was carried out by comparing the mean directions and archaeointensity values of both hearths with the SHA.DIF.14k geomagnetic field model. The results obtained are in agreement with the archaeological context, suggesting that the abandonment of the archaeological site took place between the end of ninth century and the first half of the eleventh century AD. These results provide one of the first evidences of independently well-dated sites of the Christian conquest in the Iberian northern plateau at the onset of the Early–High Middle Ages.

Keywords Archaeomagnetism · Archaeointensity · Dating methods · Magnetic properties · Secular variation

Introduction

The discovery of combustion structures such as kilns, hearths or other burnt surfaces in archaeological excavations is a good opportunity to apply the archaeomagnetic dating technique, especially if there is a lack of good chronological data. During the course of the archaeological rescue excavations carried out at La Pudia I archaeological site (Caleruega, Burgos, Northern Spain; Fig. 1), two in situ, well-preserved hearths showing signs of having experienced high-temperature heating (e.g. ashes which after excavation showed a compacted rubifacted surface) were discovered. The only chronological information available at the site comes from the typology of the pottery, which places its occupation

✉ N. García-Redondo
ngredondo@ubu.es

Á. Carrancho
acarrancho@ubu.es

M. Calvo-Rathert
mcalvo@ubu.es

Á. Palomino
angelpalomino@patrimoniointeligente.com

[1] Laboratorio de Paleomagnetismo, Dpto. Física, Universidad de Burgos, Avda Cantabria s/n, 09006 Burgos, Spain

[2] Área de Prehistoria, Departamento de Historia, Geografía y Comunicación, Universidad de Burgos, Edificio I+D+I, Plaza Misael Bañuelos s/n, 09001 Burgos, Spain

[3] Servicio Arqueomagnético Nacional y Laboratorio Interinstitucional de Magnetismo Natural (LIMNA), Instituto de Geofísica, Universidad Nacional Autónoma de México, Campus Morelia, Mexico City, Mexico

[4] Patrimonio Inteligente S.L., Carretera de Fuensaldaña s/n, 47009 Valladolid, Spain

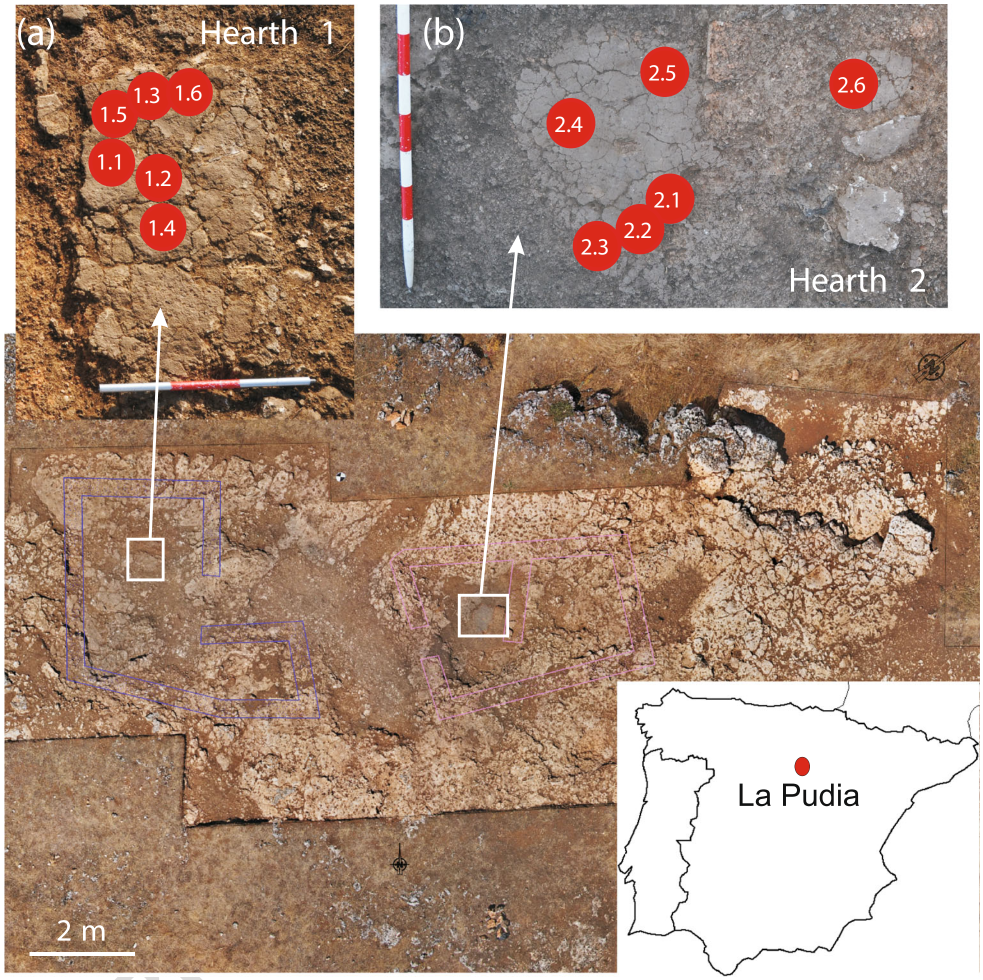

Q2 Q3 **Fig. 1** Orthomap of the archaeological site with the hearth 1 (**a**) and hearth 2 (**b**) sampled for this study indicating the location of each hand block collected. Map of the Iberian Peninsula with the location of La Pudia I archaeological site in Castile-and-León is shown

in the Middle Ages, probably around the ninth to tenth centuries AD (Aratikos Arqueólogos 2013). However, this information is based only on relative dating and a well-constrained chronological determination is needed. Hence, this discovery allowed us to perform an archaeomagnetic study in order to date the last use of both hearths and determine when the site was most likely abandoned.

Any archaeological material heated at high temperature (preferably > 500–600 °C) might be studied and potentially dated through archaeomagnetism. Heated archaeological materials contain small concentrations of ferromagnetic minerals (*s.l.*) that, under certain conditions, preserve the record of the direction and/or intensity of the Earth's magnetic field at the time of their last heating and subsequent cooling. The mechanism by which these materials record their magnetization is known as thermal remanent magnetization (TRM). This TRM is generally characterized by being parallel to the Earth's magnetic field and proportional to its intensity. Its stability over time depends on several factors such as the remanence carrying minerals, heating temperatures and duration of heating (Tauxe 2010). An important requirement to study the direction of the Earth's magnetic field is that the material under study must be in situ (preserving its position as it was cooled for the last time). However, this is not necessary to study the field intensity. Archaeomagnetic dating is applicable in those regions where there is previously a well-established master record of secular variation (SV) or a geomagnetic model covering the time period of the material being studied (e.g. Korte et al. 2009; Pavón-Carrasco et al. 2009, 2014). Furthermore, unlike other chronometric techniques such as radiocarbon, archaeomagnetism has the advantage of dating the last use (burning) and potential abandonment of the archaeological site (e.g. García-Redondo et al. 2019).

Archaeomagnetism is well established in Europe and over the last years, considerable research has been conducted in the Iberian Peninsula spanning the last millennia (e.g. Casas et al. 2014; Carrancho et al. 2013, 2017; García-Redondo et al. 2019; Gómez-Paccard et al. 2019; Hartmann et al. 2009; Molina-Cardín et al. 2018; Osete et al. 2016; Palencia-Ortas et al. 2017; Prevosti et al. 2013). Nevertheless, the amount of direction and intensity data in the Iberian Peninsula varies according to the time interval and for certain periods of the Middle Ages full vector archaeomagnetic data are still relatively scarce (Molina-Cardín et al. 2018). In spite of the efforts made so far, adding new full vector data to geomagnetic field models is necessary as the latter might not only be used for dating purposes (e.g. Pavón-Carrasco et al. 2009, 2014) but can also help to better constrain the Earth's magnetic field variations in the past.

From the historical point of view, the onset of the Early–High Middle Ages in the Iberian Peninsula is a period that coincides with the development and integration of the counties of the northern Iberian plateau giving rise to Castile simultaneously with the process of repopulation against the Andalusian power (Ladero Quesada 2014; Martín Viso 2009; Wickam 2000). The northern plateau plays an important role in this historical process and although new sites are progressively being studied (e.g. Tejerizo 2016; Ricci et al. 2018), few are really well dated by independent chronometric techniques. The objectives of this study are the following: (i) to date the last use of both hearths in order to assess if they are contemporaneous and determine the date of the site's abandonment and (ii) to provide chronological information on the historical period in which this site was occupied in the past.

Material and methods

Studied materials

The archaeological site of La Pudia I (41° 48′ 31″ N, 3° 27′ 13″ W) is located 5 km from the village of Caleruega (Burgos province), in the eastern part of Castile-and-León, in Northern Spain (Fig. 1a). Caleruega is a small medieval village founded in the tenth century AD (Aratikos Arquéologos 2013). The archaeological works at La Pudia I started in 2011 with the discovery of the remains of a building possibly dedicated for worship and three domestic areas interpreted as houses providing evidence of the coexistence of two different functional contexts. On the one hand, the possible worship space is based on a rectangular building along with a small also rectangular apse. It defines a small structure which fits well with the constructive models of the first Christian architecture in the interior of the Iberian Peninsula (Quirós Castillo 2011). On the other hand, the three domestic contexts or houses were composed of simple rectangular constructions raised with perishable materials such as wood and mud on stone basements. The material studied here consists of two hearths excavated in two different houses: hearth 1 related to house 1 and hearth 2 corresponding to house 2. According to the archaeological data mainly based on stratigraphic relationships and some local pottery fragments, both combustion structures can be considered contemporaneous and most probably related to the abandonment of the site. Various pottery fragments were recovered during the course of the excavations, indicating a chronology framed around the Early–High Middle Ages. Therefore, dating the last use of these hearths will give important information about the abandonment of the archaeological site. This was concurrent with important historical processes as the full integration of the incipient Castilian county power as well as its competition with the power of the Andalusian emirate.

Archaeomagnetic sampling

Six magnetically oriented hand-block samples were collected from each of the two hearths (Fig. 1a, b). The hand blocks were sampled by dripping plaster of Paris on them and gently pressing a piece of methacrylate on the plaster while wet, levelling it using bubble levels and allowing it to set (Lanos et al. 2005). Upon drying, the azimuth and inclination were carefully recorded with a Brunton compass. A sun compass could not be used because of the cloudy weather. Local declination error was calculated with the 12th-generation IGRF model (Thébault et al. 2015) resulting in an error of 1° W. Each hand block was later subsampled in the laboratory in order to obtain cubic specimens (~ 10 cm^3), taking into account the field orientation marks. After subsampling, we obtained 52 specimens for archaeomagnetic analyses, 22 from hearth 1 and 30 from hearth 2. Additionally, bulk samples from each hearth were collected in the field to carry out rock-magnetic and archaeointensity analyses.

Directional analyses

The directional analyses were carried out at the laboratory of palaeomagnetism of Burgos University, Spain. The natural remanent magnetization (NRM) was measured using a 2G SQUID magnetometer (noise level 5×10^{-12} Am^2). NRM was subjected to stepwise progressive alternating field (AF) and thermal (TH) demagnetization.

After conducting a pilot study to select the most appropriate demagnetization sequence, AF demagnetization was carried out in 11 steps up to a maximum peak field of 90–100 mT using the demagnetization unit of the 2G magnetometer. The TH demagnetization of the NRM was also performed in 11 steps up to a maximum temperature of 575 °C using a TD48–SC (ASC) thermal demagnetizer. Characteristic remanent magnetisation (ChRM) directions were calculated by principal component analyses (PCA) (Kirschvink 1980) of the component that linearly converges towards the origin over 5 to 8 demagnetization steps. The directional results were interpreted using the *Remasoft* software (Chadima and Hrouda 2006). The mean direction of each hearth was calculated using Fisher (Fisher 1953) statistics.

In addition, we measured the magnetic susceptibility at room temperature initially and after each thermal demagnetization step with a KLY-4 (AGICO) susceptibility meter (noise level ~ 3×10^{-8}, SI) in order to detect possible mineralogical alterations during thermal experiments in the laboratory.

Rock-magnetic analyses

Rock-magnetic analyses were also carried out at the palaeomagnetic laboratory of Burgos University to constrain the main magnetic carriers, their domain state, and their thermal stability and to preselect the best samples for palaeointensity experiments. A variable field translation balance (MM_VFTB) was used to conduct the following experiments: measurement of progressive isothermal remanent magnetization (IRM) acquisition curves, hysteresis loops (± 1 T), backfield and thermomagnetic curves up to a maximum temperature of 700 °C in air. Ten powdered samples (~ 400 mg) from both hearths were used for these analyses. The Curie temperatures (T_C) were determined in the thermomagnetic curves following the two-tangent method of Gromme et al. (1969).

The saturation magnetization (Ms), the saturation remanent magnetization (Mrs), and the coercive field (Bc) were determined from the hysteresis loops after correction for their dia- or paramagnetic fraction with the *Rock_Mag_Analyzer* software (Leonhardt 2006). The remanent coercive field (Bcr) was obtained from the backfield curves.

Archaeointensity experiments

Archaeointensity experiments were carried out using a MMTM-80 palaeointensity oven and remanence measurements were carried out using both AGICO JR5 and JR6 spinner magnetometers. For this experiment, hand blocks were fragmented into at least six specimens. In total, 30 fragments from hearth 1 and other 18 fragments belonging to hearth 2 were analysed. These fragments were pressed into salt pellets to manipulate them as standard, cylindrical palaeomagnetic samples. The absolute intensity experiments were carried out using the Thellier-type double heating method (Thellier and Thellier 1959) as modified by Coe et al. (1978). The measurements were carried out in twelve temperature steps between room temperature and 540 °C. Three control heatings at carefully selected temperature steps of 350°, 450°, and 500° (so-called pTRM checks) were performed throughout the experiments. The cooling rate dependence of TRM was investigated following a modified procedure (e.g. Morales et al. 2009) to that described by Chauvin et al. (2000), while the remanence anisotropy effect was mitigated following the procedure reported by Morales et al. (2015). The duration of slow cooling was about 7 h and 30 min while the laboratory field was set to 45 µT, with a precision better than 0.5 µT.

Results

Magnetic properties

The progressive IRM acquisition curves analysed for both hearths show that the samples are almost saturated around ~ 200 mT (> 90%) and completely saturated at 1 T, indicating that the remanence is dominated by low coercivity ferromagnetic minerals such as magnetite and/or maghemite (Fig. 2a, b).

Figure 3a–c illustrate representative examples of thermomagnetic curves (magnetization vs. temperature). The main magnetic carrier in all samples is magnetite with Curie temperatures estimated around 580 °C (Fig. 3a, b). However, these temperatures are somewhat higher in heating curves and somewhat lower in cooling curves, probably due to the relatively high heating/cooling rates of 30–40 °C/min. Occasionally, secondary magnetite is created on cooling (Fig. 3c). It should be noted that all thermomagnetic curves have the same unique component in the heating and cooling curves. Nearly all thermomagnetic curves exhibit a high reversibility (heating and cooling cycles coincide) indicating that these samples may be suitable materials for absolute archaeointensity determinations (Fig. 3a, b).

Results from thermomagnetic and IRM acquisition curves suggest that remanence of the analysed samples is carried only by magnetite. Although the interpretation of results plotted in the Day et al. (1977) diagram in terms of domain state analysis can be highly ambiguous, because hysteresis parameter ratios

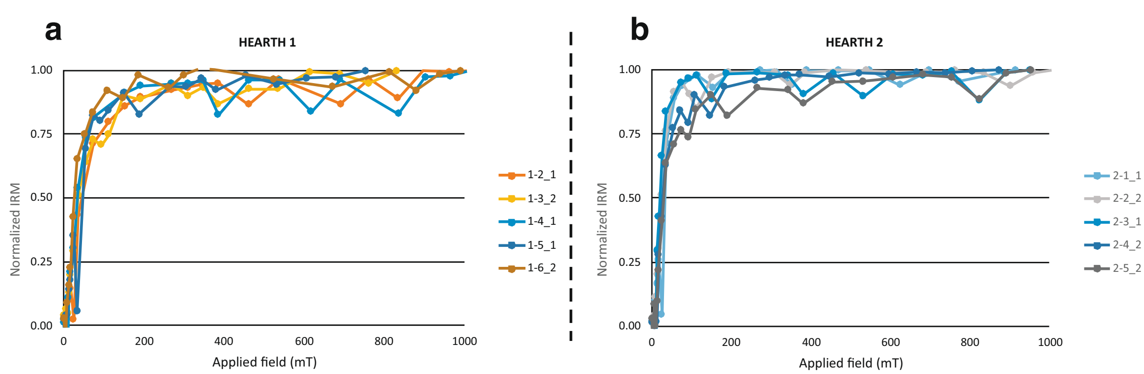

Fig. 2 Normalized progressive IRM acquisition curves up 1 T of representative samples. **a** Hearth 1. **b** Hearth 2

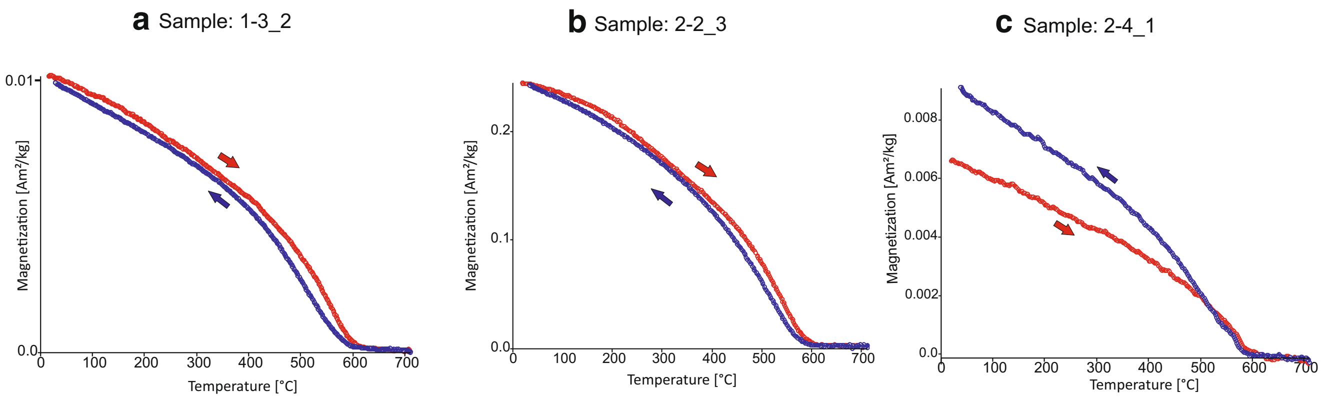

Fig. 3 Representative thermomagnetic curves from hearth 1 (**a**) and hearth 2 (**b**, **c**). Heating (cooling) cycles are indicated in red (blue) with their respective arrows. Sample code and magnetization intensities are also shown

can be influenced by several conditions (Roberts et al. 2018), the apparently simple composition of the samples from the present study may allow a qualitative interpretation. The parameter ratios of the hysteresis loops range between 0.25 < Mrs/Ms < 0.13 and 1.99 < Bcr/Bc < 4.37, indicating that the samples fall in the pseudo-single domain (PSD) area in the Day diagram (Fig. 4) (Day et al. 1977; Dunlop 2002). The samples from hearth 2 display somewhat higher Bcr/Bc values than those from hearth 1, which are closer to the single-domain (SD) area.

The high reversibility of the thermomagnetic curves and the estimated possibility of a qualitative interpretation of SD grains suggest that the samples could be useful for archaeointensity experiments.

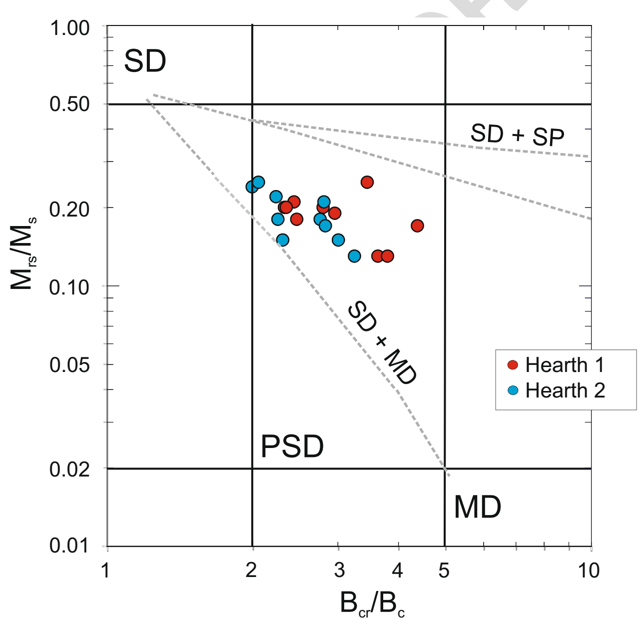

Fig. 4 Mrs/Ms vs. Bcr/Bc logarithmic plot of representative samples from hearths 1 and 2 of La Pudia I site in the Day et al. (1977) diagram according to the legend. The dashed lines represent mixing curves taken from Dunlop (2002) for mixtures of single-domain (SD) with multidomain (MD) or superparamagnetic (SP) magnetite

Archaeomagnetic directions

NRM intensities from hearth 1 lie between 3.95×10^{-6} and 1.90×10^{-4} $Am^2\ kg^{-1}$ while susceptibilities vary between 2.05×10^{-8} and 1.26×10^{-6} $m^3\ kg^{-1}$. In hearth 2, NRM intensities vary between 4.97×10^{-6} and 2.66×10^{-4} $Am^2\ kg^{-1}$ and the susceptibilities between 4.26×10^{-8} and 1.26×10^{-6} $m^3\ kg^{-1}$. The values of the Königsberger ratio [Q_n = NRM / (χH)] (Stacey 1967) were also calculated, where χ is the magnetic susceptibility and H is the intensity of the local Earth's magnetic field. This parameter helps to characterize burnt archaeological materials since it relates the induced and remanent magnetization, giving a quick estimate about the efficiency of the thermal magnetization mechanism.

In this study, the Q_n ratio values obtained range between 1.25 and 6.50 for hearth 1 and between 0.81 and 4.23 for hearth 2 (Fig. 5). In all but one case, $Q_n > 1$, confirming that the remanence is most probably of thermal origin. These values are similar to those reported for typical well-baked argillaceous materials as hearths or fireplaces (e.g. Carrancho et al. 2016, 2013; Catanzariti et al. 2012; García-Redondo et al. 2019; Gómez-Paccard et al. 2019, 2012; Schnepp et al. 2015).

Figure 6 (a–d) shows representative examples of orthogonal NRM demagnetization diagrams from the two studied hearths. Zijderveld plots of all specimens trend towards the origin during both AF and thermal treatments. The directional NRM stability and structure are similar in almost all specimens studied from both hearths. Firstly, a secondary viscous component of normal polarity easily removable at temperatures of 200–250 °C (Fig. 6a, c) or fields of 10–15 mT (Fig. 6b, d) can be distinguished. Secondly, the characteristic remanent magnetization (ChRM) direction can be isolated between 200 and 575 °C for the thermally treated specimens (Fig. 6a, c) or between 15 and 90 mT for those AF-demagnetized (Fig. 6b, d). For most specimens, approximately 50–90% of NRM is lost between the 15- and 40-mT demagnetization steps, confirming that remanence is carried by

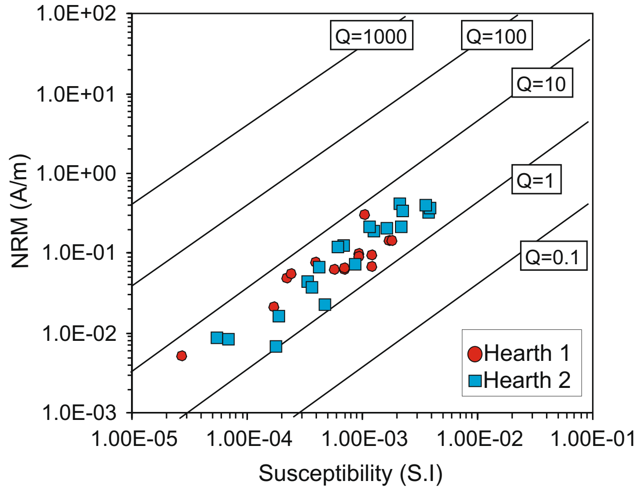

Fig. 5 Intensity of the natural remanent magnetization (NRM) versus bulk magnetic susceptibility (SI) values for all specimens from the two hearths studied. Lines indicate constant Königsberger (Q_n) values from 0.1 to 1000

low-coercivity minerals. Moreover, the median destructive field (MDF) is reached at maximum fields of 15–20 mT (Fig. 6b, d). The studied directions showed maximum angular deviation (MAD) values between 0.4 and 4.6°. Nine specimens (one from hearth 1 and eight from hearth 2) were excluded due to multicomponent NRM structure or less stable demagnetization behaviour. The excluded specimens, mostly from sample 2.6, probably underwent some process (e.g. less thermal impact or a secondary displacement) which might explain such anomalous NRM behaviour. However, there is not any evidence about it and the most conservative explanation is a sampling error. Furthermore, the majority of specimens analysed from both hearths exhibited very similar and reproducible behaviour during the demagnetization of their NRM (Fig. 6a–d).

In order to minimize the different sources of scatter commonly occurring in archaeomagnetic studies (e.g. systematic sampling errors), Lanos et al. (2005) proposed a hierarchical approach to compute and model archaeomagnetic data. The directional results obtained from both hearths are shown in Fig. 7 and in Table 1. The mean directions were calculated both at sample (hand block) and specimen levels. At a first glance, directions obtained in both hearths appear to be very similar. However, application of the test proposed by Watson (1956) indicates that it can be rejected at 95% of probability that the two populations come from the same distribution both at specimen and sample levels. Although both sample sets are statistically distinguishable, such small differences are within the intrinsic error of the method. For hearth 1, the mean direction was obtained considering 21 out of the 22 demagnetized specimens (Fig. 7a). These 21 specimens belonged to 5 different hand blocks, whose mean direction is shown in Fig. 7c. As previously said, only one specimen was rejected due to its multicomponent and less stable NRM behaviour.

With regard to hearth 2, its mean direction was calculated taking into account 22 out of 30 specimens from 5 different samples. In this case, three specimens were rejected due to multicomponent and less stable NRM structure. Sample 2.6 (from hearth 2) displayed a different mean direction ($N = 5$; declination = 343.4°; inclination = 58.7°; $\alpha_{95} = 3.8°$; $k = 400$) than the other samples from the same hearth. This sample was about 20–25 cm away from the other samples from hearth 2 (Fig. 1a), but according to archaeologists, it belonged to the same hearth (Fig. 7b, d). The possibility that the block 2.6 would have exclusively affected by some (undetermined) post-depositional process is very unlikely here and we do not have any evidence of it. Thus, the most plausible explanation for this anomalous result is a sampling error and consequently, it was excluded for the calculation of the final mean direction of hearth 2 (Fig. 7b, d and Table 1). Nonetheless, this sample was considered for archaeointensity analysis (Table 2).

Archaeointensity results

Absolute palaeointensity determinations may fail because only a limited number of burnt artefacts and independent cooling units satisfy some very specific rock-magnetic conditions necessary to be used for such determinations (see for instance Kosterov et al. 1998). Acceptance criteria for individual palaeo or archaeointensity determinations are now becoming more standardized and those used in the present study are as follows:

1. No significant deviation of NRM endpoints towards the laboratory field direction should be observed. The maximum value of γ (the angle between the ChRM and the undisturbed NRM(T) direction; Coe et al. 1984; Goguitchaichvili et al. 2015) should be below of 7°.
2. The discrepancy between control and original heating steps should lie below 15% between room temperature and 300 °C and below 10% above. Our choice is based on the fact that at the initial temperature steps, when almost no NRM demagnetization happens, larger discrepancies may be tolerated.
3. No concavity should be observed on NRM–TRM plots. In the present study, this is assessed visually.
4. Coe's quality factor q should be larger than 5.
5. The remanence fraction f used for palaeointensity determination should be more than half of the initial remanence.
6. At least 6 aligned points on the NRM decay vs. TRM acquisition curve (also known as Arai–Nagata plot) should be used for palaeointensity determination.

The cooling rate (CR) effect in the remanence acquisition was investigated following a procedure described by Chauvin et al. (2000) inducing three additional infield steps at 540 °C.

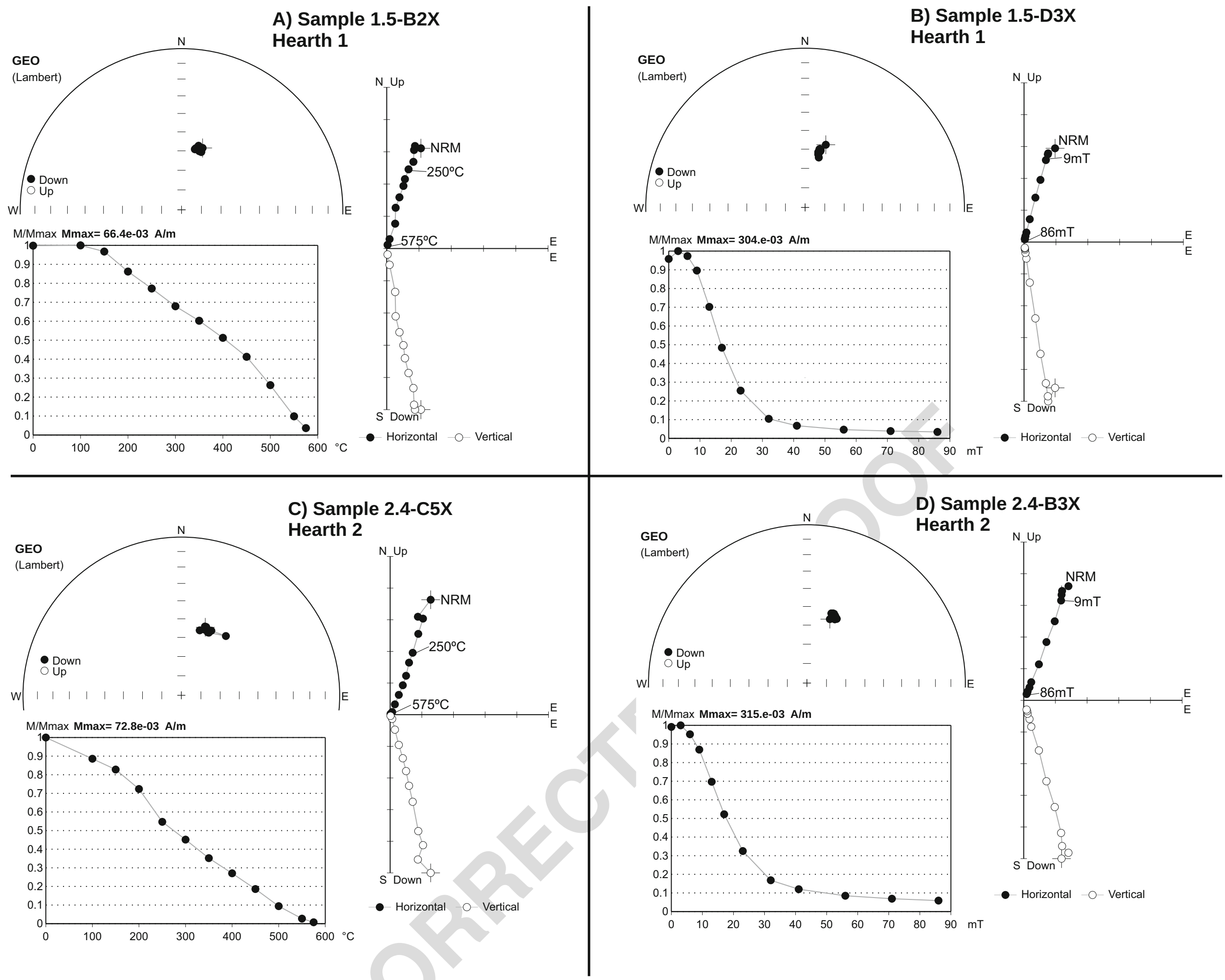

Fig. 6 Representative orthogonal NRM demagnetization diagrams showing behaviour during thermal (**a** and **c**) and alternating field (**b** and **d**) demagnetizations from hearths 1 and 2. Open (solid) symbols represent the vertical (horizontal) projections of vector endpoints. Sample code, hearth, main demagnetization steps, normalized intensity decay curves, and stereograms are shown

The first and the third heating steps (TRM1 and TRM3) were performed under the "fast" cooling conditions while the TRM2 was created with longer (natural) cooling rate. The CR ratio is related to the difference between the intensity obtained during a long (TRM2) and a short (TRM1) cooling times from 540 °C to room temperature. It should be noted that the correction is de facto only applied if the difference between first and third full thermoremanent magnetization did not exceed 10%. Under this premise, no cooling rate correction was applied to 7 samples (please see Table 2).

More than 80% of the specimens yielded technically acceptable results obeying the above-described acceptance criteria. Successful determinations are shown in Table 2. For these samples, the fraction factor f ranges between 0.59 and 0.854 and the quality factor q from 9.28 to 41.28. Figure 8(a, b) shows successful determinations while representative examples of failed experiments are reported on Fig. 8(c, d). The main reasons that explain why some archaeointensity determinations failed are due to negative pTRM checks or clearly concave Arai plots, indicating mineralogical alterations or the presence of multidomain (MD) grains, respectively. The mean archaeointensity values obtained in this study range from 46.5 to 60 μT for hearth 1 and between 51.2 and 56.1 μT for hearth 2 cooling rate corrected.

Discussion

Two mean archaeomagnetic directions and absolute archaeointensity values were obtained in the two hearths studied at sample and at specimen levels. Mean directions from both hearths are statistically undistinguishable (Fig. 7 and Table 1), well-defined, statistically robust, and suitable for

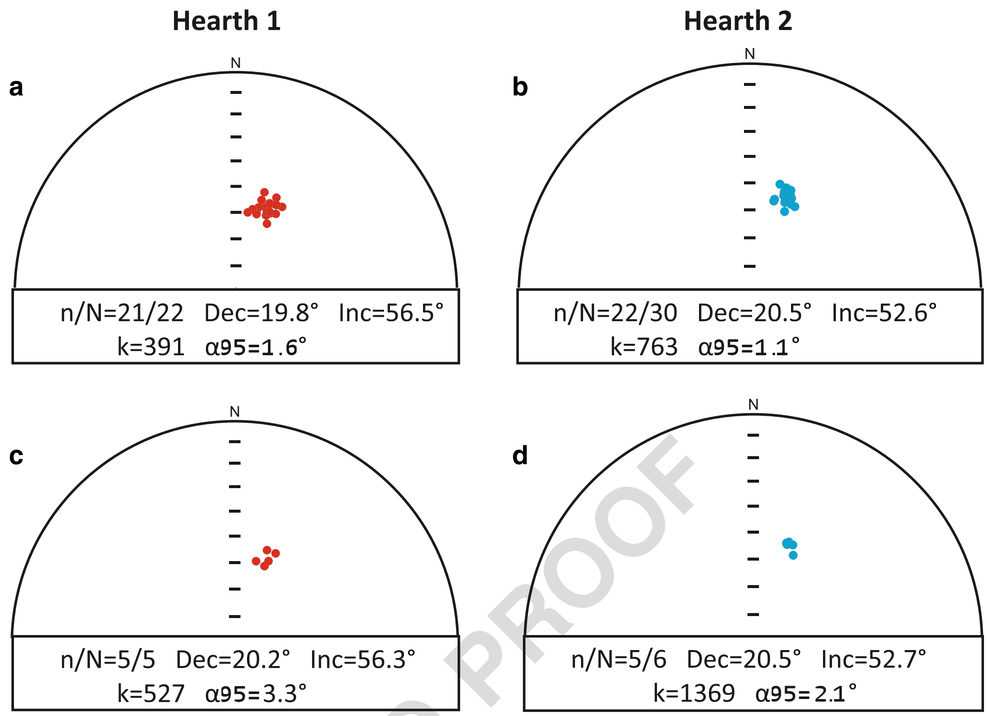

Fig. 7 Equal area projections of all ChRM directions together with the mean direction and α_{95} for hearth 1 (**a** and **c**) and hearth 2 (**b** and **d**). **a**, **b** Directional results at sample level. **d**–**f** specimen level. [n/N (n = number of samples/specimens considered for the calculation of ChRM/N = number of samples/specimens analysed); Dec, declination; Inc, inclination; α_{95}, radius of 95% confidence cone; k, precision parameter, after Fisher 1953]

carrying out an archaeomagnetic dating coupled with the archaeointensity data.

The archaeomagnetic dating method is based on the statistical comparison between the mean direction and/or intensity obtained from a burnt archaeological feature (carrying a TRM) with a previously well-constrained reference regional palaeosecular variation (PSV) curve or geomagnetic field model at the site coordinates. Once the directional (declination, D; inclination, I) and/or absolute intensity (F) mean values are determined for every studied combustion structure, the archaeomagnetic dating can be carried out using available regional SV curves or geomagnetic field models. The use of regional geomagnetic models exclusively based on independently well-dated samples carrying a TRM (e.g. Korte et al. 2009; Pavón-Carrasco et al. 2014, 2009) is especially appropriate because the latter records faithfully define

Table 1 Directional results. From left to right: [n/N] According to the description in the left column (n = number of samples or specimens taken into account to calculate the ChRM/N = number of samples or specimens analysed). D declination, I inclination. α_{95} radius of 95% confidence cone, k precision parameter according to Fisher (Fisher 1953) statistics

Q4

Archaeological structure	n/N	D (°)	I (°)	α_{95}	k
Hearth 1					
Sample level	5/5	20.2	56.3	3.3	527
Specimen level	21/22	19.8	56.5	1.6	391
Hearth 2					
Sample level	5/6	20.5	52.7	2.1	1369
Specimen level	22/30	20.5	52.6	1.1	763

the variations of the Earth's magnetic field (EMF) for the last millennia. We have used here the SHA.DIF.14k geomagnetic field model of Pavón-Carrasco et al. (2014) which describes the EMF's variations for the last 14,000 years (particularly well for the last 6 millennia) using only archaeomagnetic and lava flow data. The MATLAB® archaeomagnetic dating tool (Pavón-Carrasco et al. 2011) was used to perform the dating. It has the advantage that it calculates the variations of each geomagnetic field element at the site coordinates avoiding any relocation error which has been shown to introduce significant errors as the geographical distance increases (Casas and Incoronato 2007). Possible ages of last use of the structures will be indicated where the mean value and corresponding error of every field parameter intersects with the SV curve or geomagnetic model used. The results are shown as maps of probability density functions (PDF) and the most probable age is obtained by combining the PDF of all geomagnetic elements considered (D, I, F). In the case of multiple solutions, the choice of the most probable age interval will depend on the result being consistent with the archaeological context.

The archaeomagnetic dating of each hearth was carried out considering the three components of the magnetic field vector (declination, inclination and intensity). Figures 9 and 10 illustrate the results of the archaeomagnetic dating performed in the two hearths calculated both at sample and specimen levels. In both hearths, the dating based on hand blocks (samples) displays greater age intervals than that calculated at the specimen level. However, the difference is small, not exceeding 30 years in the case of hearth 1 and 15 years for hearth 2 (Figs. 9 and 10).

t2.1 **Table 2** Summary of archaeointensity results. T_{min}–T_{max} the temperature interval of intensity determinations, *N* the number of heating steps used, *m* slope parameter, *f* the fraction of NRM used for intensity determination, *g* the gap factor, *q* the quality factor defined by Coe et al. (1978), *B (raw)* uncorrected intensity value before anisotropy corrections, *B (corr)* archaeointensity value corrected for cooling rate effect and anisotropy effect (see text). Laboratory applied field was 45 µT

t2.2	Fragment	Cod-Lab	T_1–T_2	*N*	*m*	± sm	γ	*f*	*g*	*q*	*B* (raw)	*B* (corr)	± sB	
t2.3	Hearth 1													
t2.4	1.6	86I049	100–515	11	− 1.385	0.041	4.3	0.846	0.886	25.32	64.82	62.33	1.85	
t2.5		86I050	150–515	10	− 1.237	0.042	2.9	0.749	0.880	19.41	57.63	55.67	1.89	
t2.6		86I051	150–515	10	− 0.970	0.039	3.3	0.722	0.873	15.68	43.65*	43.65	1.76	
t2.7		86I052	150–540	11	− 1.258	0.039	5.2	0.799	0.889	22.91	59.26	56.61	1.76	
t2.8		86I053	100–540	12	− 1.167	0.040	3.1	0.854	0.893	22.25	55.34	52.52	1.80	
t2.9		86I054	100–515	10	− 1.189	0.036	2.3	0.775	0.861	22.04	54.82	53.51	1.62	
t2.10	1.1	86I055	150–540	10	− 1.406	0.057	5.8	0.753	0.874	16.23	66.29	63.27	2.57	
t2.11		86I056	150–540	11	− 1.471	0.047	6.2	0.769	0.880	21.18	67.55	66.20	2.12	
t2.12		86I057	150–540	11	− 1.331	0.035	4.3	0.713	0.873	23.67	61.51	59.90	1.58	
t2.13		86I058	150–540	11	− 1.172	0.034	5.2	0.707	0.875	21.32	54.08	52.74	1.53	
t2.14		86I059	150–515	10	− 1.408	0.049	4.2	0.755	0.873	18.94	65.32	63.36	2.21	
t2.15		86I060	150–515	10	− 1.210	0.035	4.8	0.676	0.862	20.15	57.33	54.45	1.58	
t2.16	1.5	86I067	150–515	10	− 0.924	0.034	4.3	0.664	0.874	15.77	41.58*	41.58	1.53	
t2.17		86I068	100–515	11	− 1.296	0.030	2.8	0.758	0.884	28.95	60.65	58.32	1.35	
t2.18		86I069	100–515	11	− 1.611	0.030	5.6	0.767	0.878	36.16	72.50*	72.50	1.35	
t2.19		86I070	150–515	10	− 0.821	0.037	6.0	0.646	0.847	12.14	35.82	36.95	1.67	
t2.20		86I071	100–500	10	− 1.275	0.044	5.9	0.728	0.877	18.50	59.61	57.38	1.98	
t2.21		86I072	150–515	10	− 1.319	0.022	4.4	0.739	0.871	38.59	61.23	59.36	0.99	
t2.22	1.2	86I073	150–540	11	− 1.062	0.030	5.2	0.702	0.881	21.89	49.32	47.79	1.35	
t2.23		86I074	150–515	10	− 0.900	0.042	4.9	0.598	0.853	10.93	42.11	40.50	1.89	
t2.24		86I075	150–500	9	− 0.941	0.054	7.1	0.626	0.851	9.28	42.35*	42.35	2.43	
t2.25		86I076	150–515	10	− 1.074	0.051	5.5	0.670	0.879	12.40	48.96	48.33	2.30	
t2.26		86I077	150–515	9	− 1.102	0.044	3.8	0.645	0.835	13.49	51.32	49.59	1.98	
t2.27		86I078	150–515	10	− 1.125	0.056	3.4	0.746	0.868	13.01	52.46	50.63	2.52	
t2.28										Mean=		53.7		
										±		8.9		t2.29
t2.30	Hearth 2													
t2.31	Fragment	86I079	150–500	9	− 1.242	0.064	4.5	0.836	0.862	13.98	55.89*	55.89	2.88	
t2.32		86I080	150–500	9	− 1.247	0.056	4.3	0.807	0.853	15.33	59.35	56.12	2.52	
t2.33		86I081	150–500	9	− 1.254	0.047	6.1	0.740	0.858	16.94	58.29	56.43	2.12	
t2.34		86I082	100–500	10	− 1.362	0.066	3.8	0.769	0.876	13.90	61.29*	61.29	2.97	
t2.35		86I083	150–500	9	− 1.144	0.048	5.8	0.738	0.862	15.16	52.68	51.48	2.16	
t2.36		86I084	150–515	10	− 1.227	0.057	4.6	0.753	0.862	13.97	57.13	55.22	2.57	
t2.37	2.6	86I085	150–515	10	− 1.076	0.053	3.6	0.765	0.856	13.29	50.36	48.42	2.39	
t2.38		86I086	150–515	10	− 1.361	0.021	2.7	0.739	0.862	41.28	63.52	61.25	0.95	
t2.39		86I087	150–515	10	− 1.320	0.025	4.2	0.724	0.850	32.49	60.59	59.40	1.13	
t2.40		86I088	150–515	10	− 1.254	0.044	5.4	0.681	0.848	16.46	58.23	56.43	1.98	
t2.41		86I089	150–500	9	− 1.066	0.068	3.9	0.732	0.863	9.90	47.97*	47.97	3.06	
t2.42		86I090	150–515	10	− 1.060	0.036	6.2	0.787	0.860	19.93	49.25	47.70	1.62	
t2.43	2.1	86I091	150–500	9	− 1.168	0.066	5.2	0.833	0.858	12.65	54.10	52.56	2.97	
t2.44		86I092	200–500	8	− 1.178	0.049	4.1	0.717	0.842	14.51	53.63	53.01	2.21	
t2.45		86I093	150–500	9	− 1.091	0.061	3.4	0.787	0.862	12.13	51.46	49.10	2.75	
t2.46		86I094	150–500	9	− 1.110	0.049	5.4	0.781	0.862	15.25	51.92	49.95	2.21	
t2.47		86I095	N/R											
t2.48		86I096	N/R											
t2.49										Mean =		53.9		
										±		4.6		t2.50

The easterly declination of around 20° obtained in both hearths is a characteristic feature of the Earth's magnetic field in the Iberian Peninsula between the eighth and eleventh centuries AD (Gómez-Paccard et al. 2006; Molina-Cardín et al. 2018). This variation is especially diagnostic for the dating and implies that in all cases only a single age interval is obtained, regardless of whether it is calculated at the sample or at the specimen level. The most probable age interval at a sample

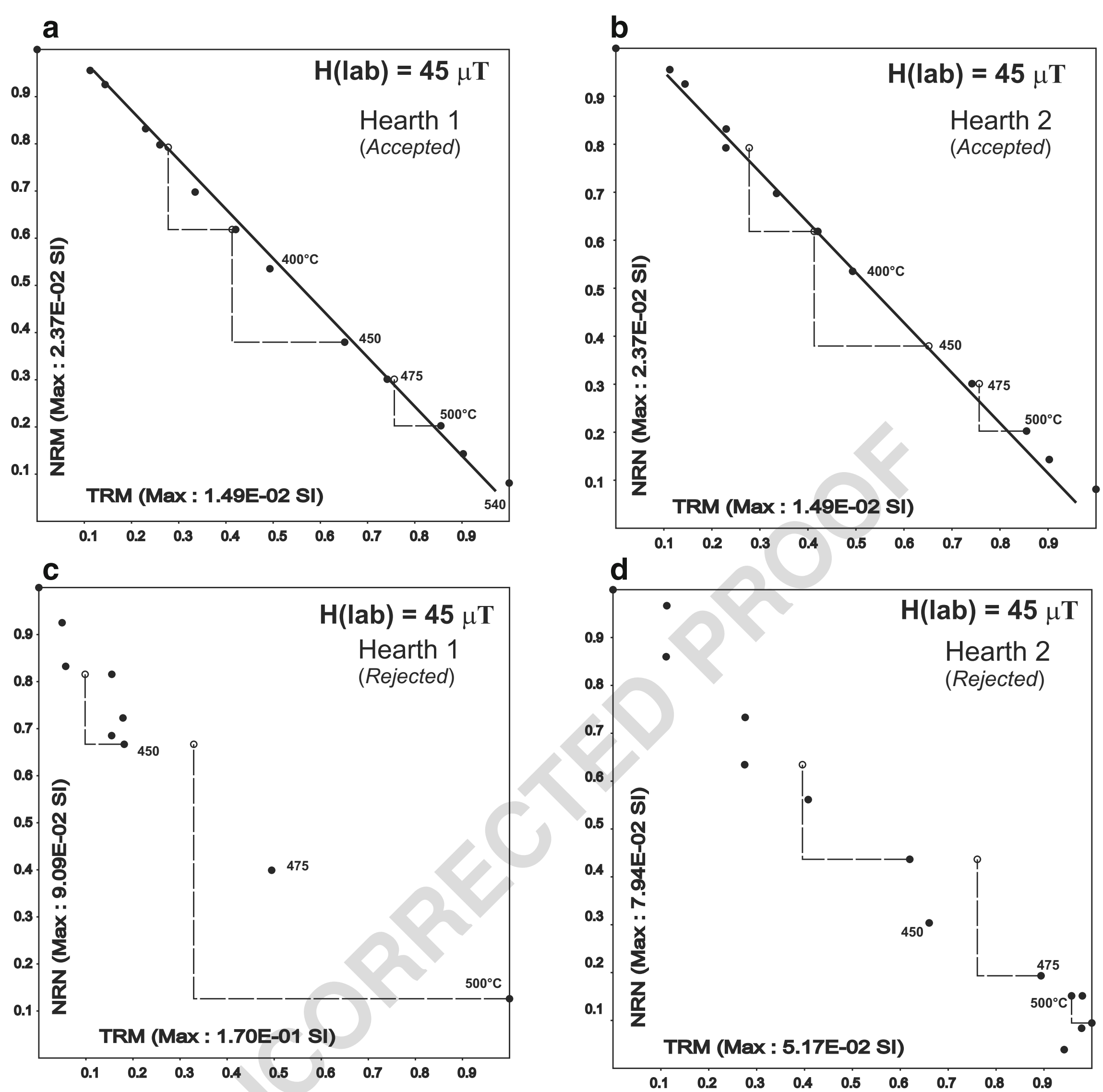

Fig. 8 Representative NRM–TRM plots (so-called Arai–Nagata plots) for representative samples of the studied hearths. **a**, **b** Two successful determinations. **c**, **d** Two rejected determinations (see also Table 2)

level for hearth 1 is 852–1063 AD and in the case of hearth 2 it is 987–1074 AD, both at 95% confidence level (Figs. 9a and 10a, respectively). Archaeomagnetic dating performed at the specimen level suggests that the last use of hearth 1 most probably took place between 866 and 1048 AD whereas in hearth 2 it took place between 995 and 1067 AD, both at the 95% probability level (Figs. 9b and 10b, respectively). These results suggest that the abandonment of both hearths occurred almost simultaneously or closely confined in time between the end of ninth century and the first half of the eleventh century AD.

These dating results are in good agreement with the archaeological context. The archaeological materials recovered mainly focus on ceramic remains of local production. Among the ceramic collection, a vessel painted with linear geometric motifs in vinous tones stands out, which is possibly associated with the elites of the incipient Castilian county power and whose consolidation takes place between the ninth and tenth century AD (Aratikos Arqueólogos 2013). Most likely, the La Pudia I archaeological site represents an example of this historical process in the northern half of the Iberian Peninsula. According to the typological and decorative characteristics of the ceramics recovered at La Pudia, the archaeologists date the abandonment of the site between the ninth and tenth century AD and estimate that the hill was with all probability abandoned at the beginning of eleventh century AD (Aratikos Arqueólogos 2013). This is in good agreement with the archaeomagnetic dating results reported here. This process of county consolidation in Castile is also concurrent with the beginning of the repopulation along the Duero River after the Muslim invasion (Barrios García 1985; Carvajal Castro and Martín Viso 2013; López Quiroga and Rodríguez

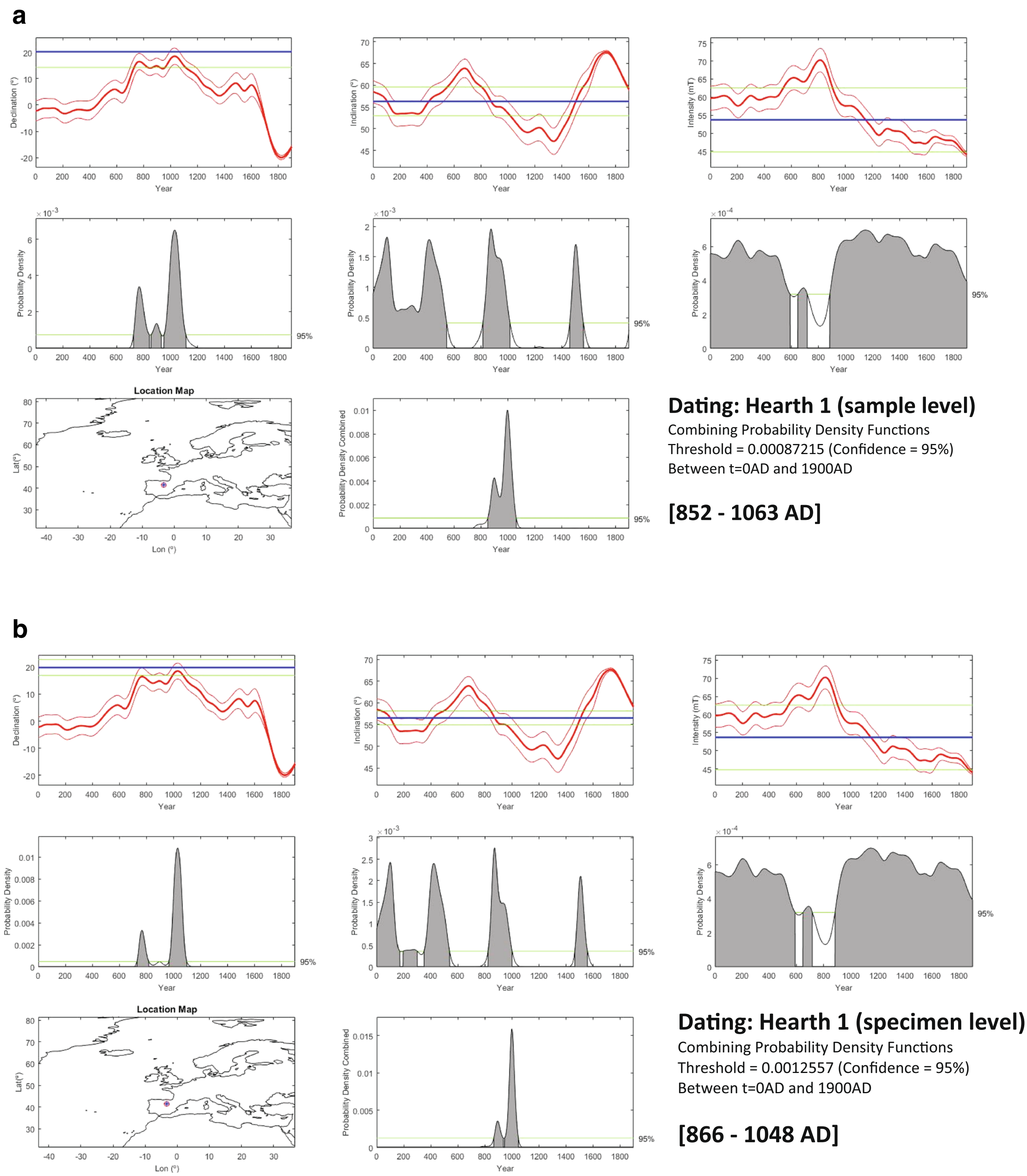

Fig. 9 Archaeomagnetic dating results obtained for hearth 1. Age probability density functions obtained with the MATLAB® tool of Pavón-Carrasco et al. (2011) comparing the SHA.DIF.14k model with the declination (left), inclination (middle) and intensity values (right) at site coordinates from hearth 1. Results are expressed at 95% probability. **a** The results at the sample level. **b** The results at the specimen level

Lovelle 1991). The Castilian county power would enter into competition with the Al-Ándalus emiral power during the tenth century AD performing in this area several military campaigns, in order to slow down the political consolidation of Christian advancement, rather than a real submission of this area and its integration into the political structure of Al-

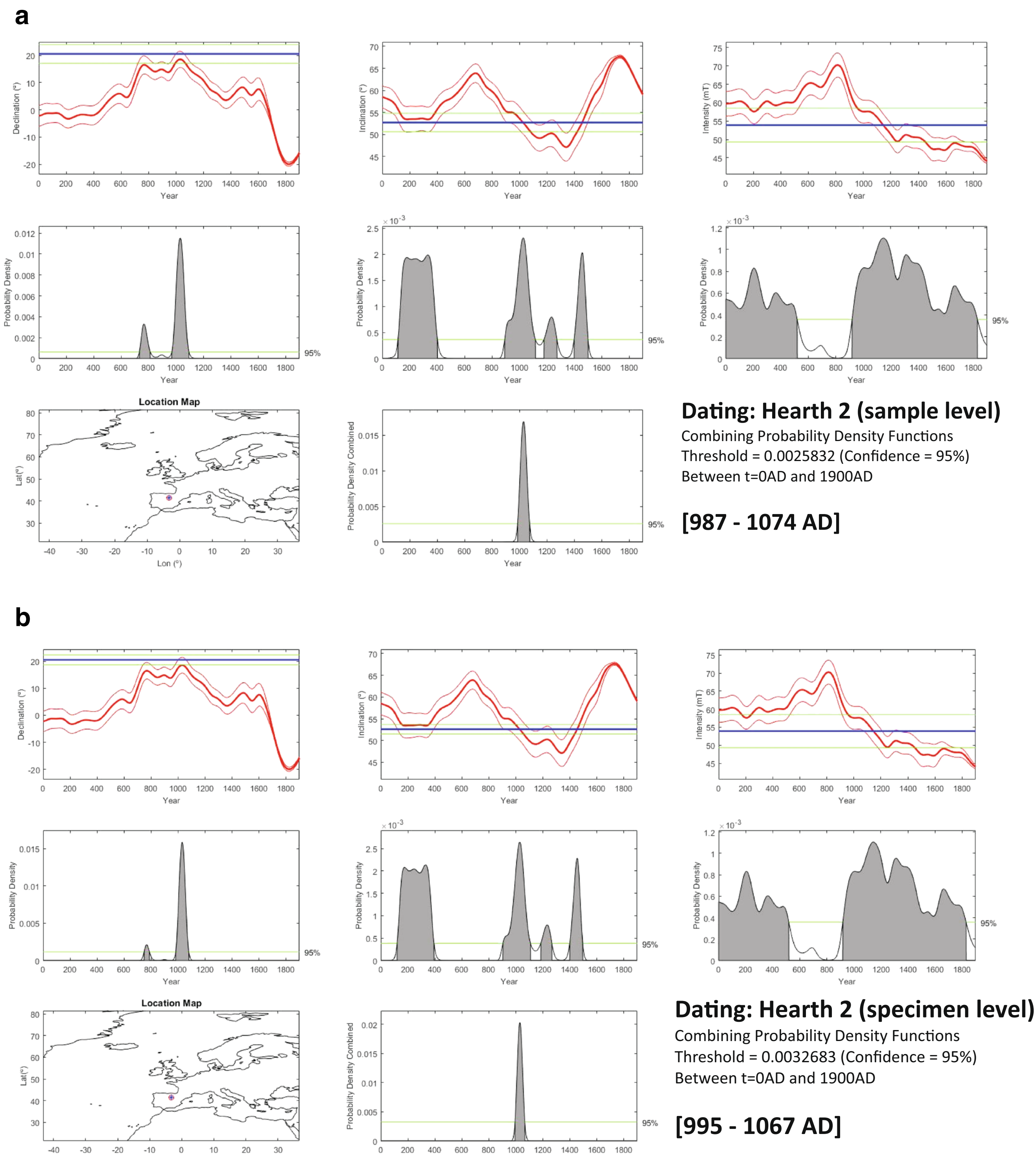

Fig. 10 Archaeomagnetic dating results obtained for hearth 2. **a** The results at the sample level. **b** The results at the specimen level. Results are expressed at 95% probability

Andalus (Martínez Díez 2005). In summary, these archaeomagnetic dates provide reliable chronological information to an important historical process in which systematic dating of archaeological sites is highly necessary.

Conclusions

A full vector archaeomagnetic dating was carried out on two hearths from the Early–High Middle Ages archaeological site of La Pudia I (Caleruega, Burgos, Spain). The following conclusions can be drawn:

1. Most studied samples are suitable for absolute archaeointensity determinations, as shown by palaeomagnetic and rock-magnetic results: The main magnetic carrier is Ti-poor titanomagnetite in PSD state and most samples from both hearths display reversible thermomagnetic curves.
2. Two statistically robust mean directions from both hearths were obtained with $\alpha_{95} < 3°$ and k values are over 400. Mean directions were calculated in the two hearths both at sample and at specimen levels, showing very similar results but statistically distinguishable at 95% confidence level.
3. 40 successful absolute archaeointensity determinations were obtained from specimens from both hearths. After anisotropy correction, the mean archaeointensity value for hearth 1 yields 53.7 ± 8.9 μT and for hearth 2, 53.9 ± 4.6 μT.
4. The comparison of the mean directional and intensity values from both hearths with the SHA.DIF.14k geomagnetic model resulted in different age intervals of last use at the 95% confidence level. For hearth 1 (at the sample level), 852–1063 AD and 866–1048 AD (at the specimen level). For hearth 2 (at the sample level), 987–1075 AD and 995–1067 AD (at the specimen level).
5. These dates perfectly agree with the archaeological context, indicating that the last use of both hearths and subsequent abandonment of the site occurred almost simultaneously or closely confined in time between the end of ninth century and the first half of the eleventh century AD. This is the only chronometric dating available for the site so far. These results provide important new data to one of the least known and most poorly dated archaeological horizons during the Early–High Middle Ages in the Northern Iberian Peninsula.

Acknowledgements Thanks to the archaeological team who worked at the site. Orthophoto shown in Fig. 1 was done by Aratikos Arqueólogos.

Funding information N-G.R. acknowledges the financial support given by the Junta de Castilla y León and the European Union (ERDF). This study was funded by the project BU235P18 of the Junta de Castilla y León and the European Regional Development Fund (ERD). The archaeological works were carried out with the economic support of the city council of Caleruega.

References

Aratikos Arqueólogos SL (2013) Intervención arqueológica previa al desarrollo del Proyecto de Puesta en Valor de los recursos del Patrimonio Arqueológico de Caleruega (Burgos). Excavación en el yacimiento de "La Pudia I". Informe Técnico. 212 pp.

Barrios García Á (1985) Repoblación en la zona meridional del Duero: Fases de ocupación, procedencias y distribución espacial de los grupos repobladores. Studia Histórica: Historia Medieval 3:33–82

Carrancho A, Villalaín JJ, Pavón-Carrasco FJ, Osete ML, Straus LG, Vergès JM, Carretero JM, Angelucci DE, González-Morales MR, Arsuaga JL, Bermúdez de Castro JM, Carbonell E (2013) First directional European palaeosecular variation curve for the Neolithic based on archaeomagnetic data. Earth Planet Sci Lett 380:124–137. https://doi.org/10.1016/j.epsl.2013.08.031

Carrancho Á, Herrejón-Lagunilla Á, Vergès JM (2016) Three archaeomagnetic applications of archaeological interest to the study of burnt anthropogenic cave sediments. Quat Int 414:244–257. https://doi.org/10.1016/j.quaint.2015.10.010

Carrancho Á, Goguitchaichvili A, Morales J, Espinosa-Sota JA, Villalaín JJ, Arsuaga JL, Baquedano E, Pérez-González A (2017) Full-vector archaeomagnetic dating of a medieval limekiln at Pinilla Del Valle site (Madrid, Spain). Archaeometry 59(2):373–394

Carvajal Castro Á, Martín Viso I (2013) Historias regionales de la repoblación: los reyes asturleoneses y las "políticas de la tierra" en el oeste de la Meseta. In: del Duero P, De La Cruz Díaz F, Luis Corral y I, Viso M (eds) El historiador y la sociedad. Universidad de Salamanca, Salamanca, pp 39–52

Casas L, Prevoosti M, Fouzai B, Álvarez A (2014) Archaeomagnetic study and dating at five sites from Catalonia (NE Spain). J Archaeol Sci 41:856–867. https://doi.org/10.1016/j.jas.2013.10.020

Casas L, Incoronato A (2007) Distribution analysis of errors due to relocation of geomagnetic data using the "conversion via pole" (CVP) method: implications on archaeomagnetic data. Geophys J Int 169:448–454. https://doi.org/10.1111/j.1365-246X.2007.03346.x

Catanzariti G, Gómez-Paccard M, Mcintosh G, Pavón-Carrasco FJ, Chauvin A, Osete ML (2012) New archaeomagnetic data recovered from the study of Roman and Visigothic remains from Central Spain (3rd-7th centuries). Geophys J Int 188:979–993. https://doi.org/10.1111/j.1365-246X.2011.05315

Chadima M, Hrouda F (2006) Remasoft 3.0 a user-friendly palaeomagnetic databrowser and analyzer. Trav Geophys XXVII:20–21

Chauvin A, García Y, Lanos P, Laubenheimer F (2000) Paleointensity of the geomagnetic field recovered on archaeomagnetic sites from France. Phys Earth Planet Inter 120:111–136

Coe RS, Grommé S, Mankinen EA (1978) Geomagnetic paleointensities from radiocarbon- dated lava flows on Hawaii and the question of the Pacific non-dipole low. J Geophys Res 83(B4):1740–1756. https://doi.org/10.1029/JB083iB04p01740

Coe RS, Gromme S, Mankinen EA (1984) Geomagnetic paleointensities from excursion sequences in lavas on Oahu, Hawaii. J Geophys Res Solid Earth. https://doi.org/10.1029/JB089iB02p01059

Day R, Fuller M, Schmidt VA (1977) Hysteresis properties of titanomagnetites: grain-size and compositional dependence. Phys Earth Planet Inter 13:260–267. https://doi.org/10.1016/0031-9201(77)90108-X

Dunlop DJ (2002) Theory and application of the Day plot (Mrs/Ms versus Hcr/Hc) 1. Theoretical curves and tests using titanomagnetite data. J Geophys Res 107:EPM4–1–EPM4–22. https://doi.org/10.1029/2001JB000486

Fisher R (1953) Dispersion on a sphere. Proc R Soc A Math Phys Eng Sci 217:295–305. https://doi.org/10.1098/rspa.1953.0064

García-Redondo N, Carrancho Á, Goguitchaichvili A, Morales J, Palomino A (2019) Comprehensive magnetic surveys of kilns for bell and tile fabrication in Castile (Spain). J Archaeol Sci Rep 23:426–436. https://doi.org/10.1016/j.jasrep.2018.11.003

Goguitchaichvili A, Morales J, Schavelzon D, Vásquez C, Gogorza C, Loponte D, Rapalini A (2015) Variation of the Earth's magnetic field strength in South America during the last two millennia: new results from historical buildings of Buenos Aires and re-evaluation of regional data. Phys Earth Planet Inter 245:15–25

Gómez-Paccard M, Chauvin A, Lanos P, McIntosh G, Osete ML, Catanzariti G, Ruiz-Martínez VC, Núñez JI (2006) First archaeomagnetic secular variation curve for the Iberian Peninsula: comparison with other data from western Europe and with global geomagnetic field models. Geochemi Geophys Geosyst 7. https://doi.org/10.1029/2006GC001476

Gómez-Paccard M, McIntosh G, Chauvin A, Beamud E, Pavón-Carrasco FJ, Thiriot J (2012) Archaeomagnetic and rock magnetic study of six kilns from North Africa (Tunisia and Morocco). Geophys J Int 189:169–186. https://doi.org/10.1111/j.1365-246X.2011.05335.x

Gómez-Paccard M, Rivero-Montero M, Chauvin A, García i Rubert D, Palencia-Ortas A (2019) Revisiting the chronology of the Early Iron Age in the North-Eastern Iberian Peninsula. Archaeol Anthropol Sci 11:4755–4767. https://doi.org/10.1007/s12520-019-00812-9

Gromme CS, Wright TL, Peck DL (1969) Magnetic properties and oxidation of iron-titanium oxide minerals in Alae and Makaopuhi Lavalakes, Hawaii. J Geophys Res 74:5277

Hartmann GA, Trindade RIF, Goguitchaichvili A, Etchevarne C, Morales J, Afonso MC (2009) First archeointensity results from Portuguese potteries (1550–1750 AD). Earth Planets Space 61(1):93–100

Kirschvink JL (1980) The least-square line and plane and the analysis of paleomagnetic data. Geophys J R Astron Soc 62:699–718

Korte M, Donadini F, Constable CG (2009) Geomagnetic field for 0–3 ka: 2. A new series of time-varying global models. Geochem Geophys Geosyst 10. https://doi.org/10.1029/2008GC002297

Kosterov AA, Perrin M, Glen JM, Coe RS (1998) Paleointensity of the Earth's magnetic field in Early Cretaceous time: the Parana Basalt, Brazil. J Geophys Res 103(B5):9739–9753. https://doi.org/10.1029/98JB00022

Ladero Quesada, M Á (2014) La formación medieval de España. ISBN 978-84-206-8736-0

Lanos P, Le Goff M, Kovacheva M, Schnepp E (2005) Hierarchical modelling of archaeomagnetic data and curve estimation by moving average technique. Geophys J Int 160:440–476. https://doi.org/10.1111/j.1365-246X.2005.02490.x

Leonhardt R (2006) Analyzing rock magnetic measurements: the RockMagAnalyzer 1.0 software. Comput Geosci 32:1420–1431. https://doi.org/10.1016/j.cageo.2006.01.006

López Quiroga J, Rodríguez Lovelle M (1991) Una aproximación arqueológica al problema historiográfico de la "despoblación y repoblación en el valle del Duero" s.VIII-XI. Anu Estud Mediev 21:3–10

Martín Viso I (2009) Tiempos oscuros? Territorios y sociedad en el centro de la Península Ibérica (siglos VII-X), Madrid

Martínez Díez G (2005) El Condado de Castilla (711–1038). La historia frente a la leyenda. II vols. Valladolid

Molina-Cardín A, Campuzano SA, Osete ML, Rivero-Montero M, Pavón-Carrasco FJ, Palencia-Ortas A, Martín-Hernández F, Gómez-Paccard M, Chauvin A, Guerrero-Suárez S, Pérez-Fuentes JC, McIntosh G, Catanzariti G, Sastre Blanco JC, Larrazabal J, Fernández Martínez VM, Álvarez Sanchís JR, Rodríguez-Hernández J, Martín Viso I, Garcia i Rubert D (2018) Updated Iberian archeomagnetic catalogue: new full vector paleosecular variation curve for the last three millennia. Geochem Geophys Geosyst 19:3637–3656. https://doi.org/10.1029/2018GC007781

Morales J, Goguitchaichvili A, Acosta A, González T, Alva-Valdivia L, Robles-Camacho J, Hernández-Bernal MS (2009) Magnetic properties and archeointensity determination on pre Columbian pottery from Chiapas, Mesoamerica. Earth Planets Space Special Issue 61: 83–91

Morales J, Fernández Martínez G, Goguitchaichvili A, Cárdenas E, Herández Bernal MS (2015) Archeomagnetic dating of some pre-Columbian pottery fragments from northern Mesoamerica: implications for the chronology of Central Mexico during the Epiclassic period. J Archaeol Sci Rep 4:32–43

Osete ML, Chauvin A, Catanzariti G, Jimeno A, Campuzano SA, Benito-Batanero JP, Tabernero-Galán C, Roperch P (2016) New archaeomagnetic data recovered from the study of celtiberic remains from Central Spain (Numantia and Ciadueña, 3rd−1st BC). Implications on the fidelity of the Iberian palaeointensity database. Phys Earth Planet Inter 260:74–86

Palencia-Ortas A, Osete ML, Campuzano SA, Mcintosh G, Larrazabal J, Sastre L, Rodríguez-Aranda J (2017) New archaeomagnetic directions from Portugal and evolution of the geomagnetic field in Iberia from Late Bronze Age to Roman times. Phys Earth Planet Inter 270: 183–194. https://doi.org/10.1016/j.pepi.2017.07.004

Pavón-Carrasco FJ, Osete ML, Torta JM, Gaya-Piqué LR (2009) A regional archeomagnetic model for Europe for the last 3000 years, SCHA.DIF.3K: applications to archeomagnetic dating. Geochem Geophys Geosyst 10:1–22. https://doi.org/10.1029/2008GC002244

Pavón-Carrasco FJ, Rodríguez-González J, Osete ML, Miguel J (2011) A Matlab tool for archaeomagnetic dating. J Archaeol Sci 38:408–419

Pavón-Carrasco FJ, Osete ML, Torta JM, De Santis A (2014) A geomagnetic field model for the Holocene based on archaeomagnetic and lava flow data. Earth Planet Sci Lett 388:98–109. https://doi.org/10.1016/j.epsl.2013.11.046

Prevosti M, Casas LI, Roig-Perez JF, Fouzai B, Alvarez A, Pitarch A (2013) Archaeological and archaeomagnetic dating at a site from the ager Tarraconensis (Tarragona, Spain): El Vila-sec Roman pottery. J Archaeol Sci 40:2686–2701. https://doi.org/10.1016/j.jas.2013.01.027

Quirós Castillo JA (2011) La arquitectura doméstica en los yacimientos rurales en torno al año 711. en Zona Arqueológica II:63–82

Ricci P, García-Collado MI, Narbarte Hernández J, Grau Sologestoa I, Quirós Castillo JA, Lubritto C (2018) Chronological characterization of medieval villages in Northern Iberia: a multi-integrated approach. Eur Phys J Plus 133:133–110. https://doi.org/10.1140/epjp/i2018-12233-5

Roberts AP, Tauxe L, Heslop D, Zhao X, Jiang ZX (2018) A critical appraisal of the "Day diagram". J geophysRes Solid Earth 123(4): 2618–2644. https://doi.org/10.1002/2017JB015247

Schnepp E, Obenaus M, Lanos P (2015) Posterior archaeomagnetic dating: an example from the Early Medieval site Thunau am Kamp, Austria. J Archaeol Sci Rep 2:688–698. https://doi.org/10.1016/j.jasrep.2014.12.002

Stacey FD (1967) The Koenigsberger ratio and the nature of thermoremanence in igneous rocks. Earth Planet Sci Lett 2:67–68. https://doi.org/10.1016/0012-821X(67)90174-4

Tejerizo C (2016) Arqueología del campesinado medieval en la Cuenca del Duero (ss. V-VIII D.C). Tesis doctoral. Universidad del País Vasco

Tauxe L (2010) Essentials of paleomagnetism. University of California Press, Berkeley, p 516

Thébault E, Finlay CC, Beggan CD et al (2015) International geomagnetic reference field: the 12th generation. Earth Planet Space 67:79. https://doi.org/10.1186/s40623-015-0228-9

Thellier E, Thellier O (1959) Sur l'intensité du champ magnétique terrestre dans le passé historique et géologique. Ann Geophys 15: 285–376

Watson GS (1956) Analysis of dispersion on a sphere. Mon Not Astr Soc Geophys Suppl 7:153–159

Wickam C (2000) Overview: production, distribution and demand, II, I. L. Hansen Y, Wickham C (Eds.), The long eight century, Leiden, Brill, pp. 345-377

AUTHOR QUERIES

AUTHOR PLEASE ANSWER ALL QUERIES.

Q1. Please check if the affiliations are presented correctly.
Q2. Please check if the figure captions are correctly presented.
Q3. Figure 9,10 contains poor quality and small text inside the artwork. Please do not re-use the file that we have rejected or attempt to increase its resolution and re-save. It is originally poor, therefore, increasing the resolution will not solve the quality problem. We suggest that you provide us the original format. We prefer replacement figures containing vector/editable objects rather than embedded images. Preferred file formats are eps, ai, tiff and pdf.
Q4. Please check if data reflected inside the tables are correctly presented.